THE JOURNAL OF PHYSICAL CHEMISTRY Letters

Letter

pubs.acs.org/JPCL

Dynamic Microscopy Study of Ultrafast Charge Transfer in a Hybrid P3HT/Hyperbranched CdSe Nanoparticle Blend for Photovoltaics

Giulia Grancini,*[,†,#] Mariano Biasiucci,[‡,§] Rosanna Mastria,[⊥] Francesco Scotognella,*[,†] Francesco Tassone,[#] Dario Polli,[†] Giuseppe Gigli,[⊥,∥] and Guglielmo Lanzani[†,#]

[†]Dipartimento di Fisica, Politecnico di Milano, Piazza L. da Vinci, 32, 20133 Milano, Italy

[‡]NNL-CNR Nanoscience Institute c/o Dip. Fisica Ed. G. Marconi, La Sapienza University, Roma, Italy

[§]Electronical Engineering Department, Tor Vergata University, Via del Politecnico, 00133 Roma, Italy

[⊥]NNL-CNR Nanoscience Institute, Dip. Ingegneria Innovazione, Università del Salento, via Arnesano, 73100 Lecce, Italy

[#]Center for Nano Science and Technology @ PoliMi, Istituto Italiano di Tecnologia, Via Pascoli 70/3, 20133 Milano, Italy

[∥]CNR, Ist Nanosci, NNL, I-73100 Lecce, Italy

Supporting Information

ABSTRACT: We present a spectroscopic investigation on a new hyperbranched cadmium selenide nanocrystals (CdSe NC)/poly(3-hexylthiophene) (P3HT) blend, a potentially good active component in hybrid photovoltaics. Combined ultrafast transient absorption spectroscopy and morphological investigations by means of an ultrafast confocal microscope reveal a strong influence of the complex local structure on the photogenerated carrier dynamics. In particular, we map the electron-transfer process across the hybrid NC/polymer interface, and we reveal that charge separation occurs through a preferential pathway from the CdSe nanobranches to the P3HT chains. Efficient charge generation at the distributed heterojunction is also confirmed by scanning kelvin probe force microscopy measurements.

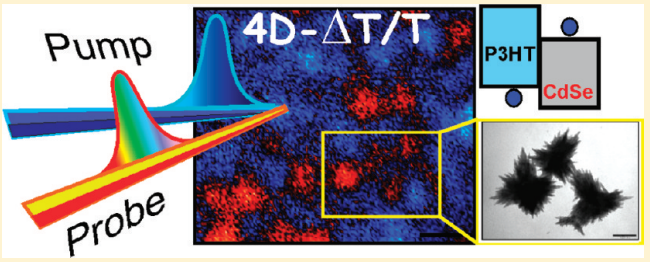

SECTION: Kinetics, Spectroscopy

Hybrid composites mixing semiconductor nanocrystals (NC) with conjugated polymers are attractive materials for future-generation photovoltaics.[1−4] They combine the easy processability and cheapness of plastic materials with the high charge mobility and tunable optical and morphological properties of inorganic NCs. In photovoltaic blends for solar cell applications, the charge separation and extraction processes are typically dictated by the degree of phase separation. To maximize their efficiency, a balanced compromise must be found between the large interfacial area required for charge photogeneration, requiring small-phase domains, and the number and topology of the interconnections leading to percolating transport, calling for partial domain clustering.[5,6] Hybrid organic/NC blends could bring an advantage in this regard because their preordered geometry leads to high interfacial area while preserving collection paths.[7] Different NC architectures have been proposed, such as dots, nanorods, and three-dimensional branched nanoparticles.[8,9] The latter reached power conversion efficiency above 2%,[8−16] which has been attributed to the higher interfacial area and improved percolation paths with respect to quantum dots/polymer films.[8,9]

Here, we incorporate a new type of three-dimensional hyperbranched colloidal CdSe NC with regioregular P3HT forming a bicontinuous and nanoscopic phase-separated blend. This system allows us to investigate the effect of the branching strategy on the dynamics of the photoinduced carriers.[17−20] To perform this study, we apply the ultrafast four-dimensional (4D) microscopy technique[21] to image femtosecond differential transmission ($\Delta T/T(\lambda,\tau)$) signals in the blend. We obtain detailed information on the relaxation pathways of photoexcited species both within the CdSe hyperbranched NC and across the different phases of the heteromaterials. Knowledge about carrier dynamics from the earliest events of photoexcitation provides a hint for understanding device performance limitations.[15−17]

The inset of Figure 1a presents the transmission electron micrographs (TEMs) of the hyperbranched CdSe NC, showing the typical dendritic structure with many branching points, allowing control of the dispersion of the inorganic phase in the polymer matrix. This provides a large, distributed surface area for driving charge separation at the interface with another material.[19] The CdSe NC exhibit a broad-band absorption (red dotted line in Figure 1a) covering the whole visible range up to 710 nm, while the P3HT has a complementary absorption

Received: January 10, 2012
Accepted: February 1, 2012
Published: February 1, 2012

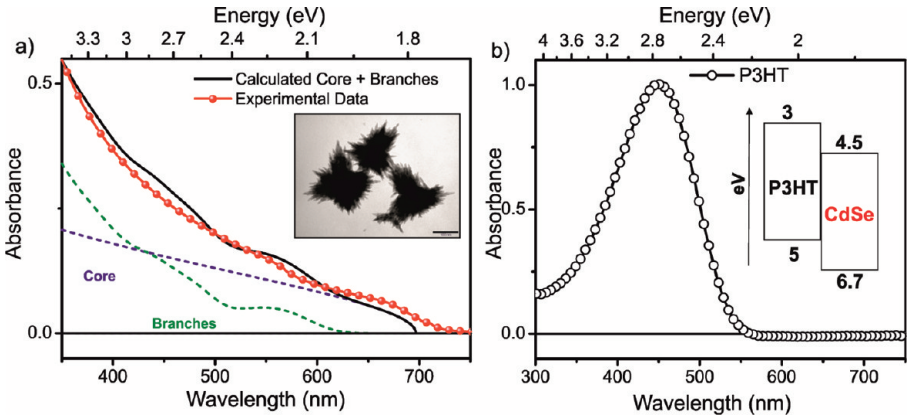

Figure 1. (a) Measured (red dotted line) and calculated (black solid line) absorption spectrum of CdSe. Green dashed line: calculated optical absorption of the rods (branches); blue dashed line: calculated optical absorption of the spherical seed cores. In the inset is the TEM image of hyperbranched shaped CdSe NC after synthesis and purification; scale bar = 100 nm. (b) Absorption spectrum of pristine P3HT. In the inset, a cartoon of the energetic levels of the P3HT and the NC is presented.

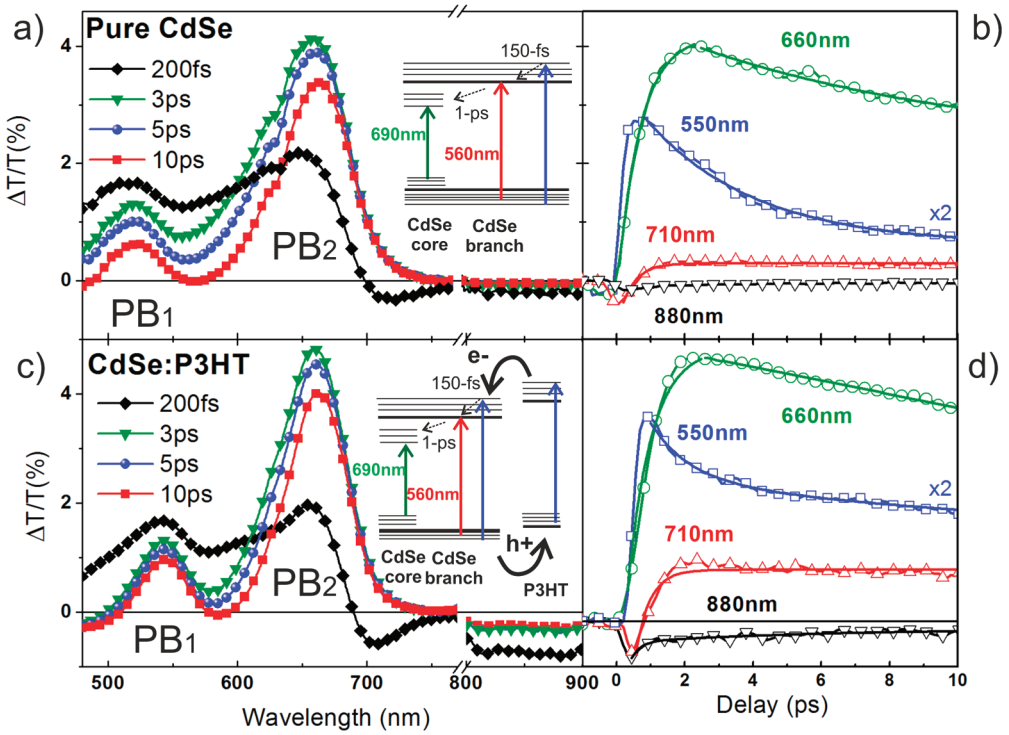

Figure 2. $\Delta T/T(\lambda)$ spectra of (a) pure CdSe NC and (c) of a 1:1 w/w P3HT/CdSe blend. Scheme of the energetic levels in the inset. $\Delta T/T(\tau)$ at selected probe wavelengths of pure CdSe NC (b) and of a 1:1 w/w P3HT/CdSe blend (d).

spectrum, exhibiting a maximum at around 500 nm (black line in Figure 1b). In particular, the absorption spectrum of the CdSe shows a major peak at 1.8 eV (680 nm) and a knee at around 2.2 eV (560 nm). In order to assign these two main features, we modeled the hyperbranched NC as spherical seeds of about 10 nm diameter over which rods several tens of nanometers long were grown. Alternative structures based on small seeds with protruding tapered branches, as suggested by TEM images of a few branched structures (tetrapods, octapods), would not result in good agreement of the modeled and the measured absorption spectra and were thus not further considered. This picture is consistent with the architecture and growth mechanism proposed by Alivisatos et al. in ref 9. In particular, we modeled the optical absorption from rods (green dashed line in Figure 1a) by varying their diameters in order to fit the higher-energy feature, using the effective mass approximation solved with a finite element method and considering both heavy and light holes.[19] The absorption from the large spherical seeds (blue dashed line in Figure 1a) is instead modeled as absorption from a bulk semiconductor with parabolic bands. The agreement with the experimental data is reasonable in view of the simplified assumption made for both the complex architecture and structure of the bands and states of the CdSe bulk and nanorods. The difference between the energy gap of the CdSe seed and that of the branches is on the order of 400 meV. From this simple model, we infer that the volume ratio of the large spherical seeds and nanorods is about 1. We notice that no spherical seed is evident in the TEM image as it is probably hidden by the dense network of rods.

dx.doi.org/10.1021/jz3000382 | J. Phys. Chem. Lett. 2012, 3, 517–523

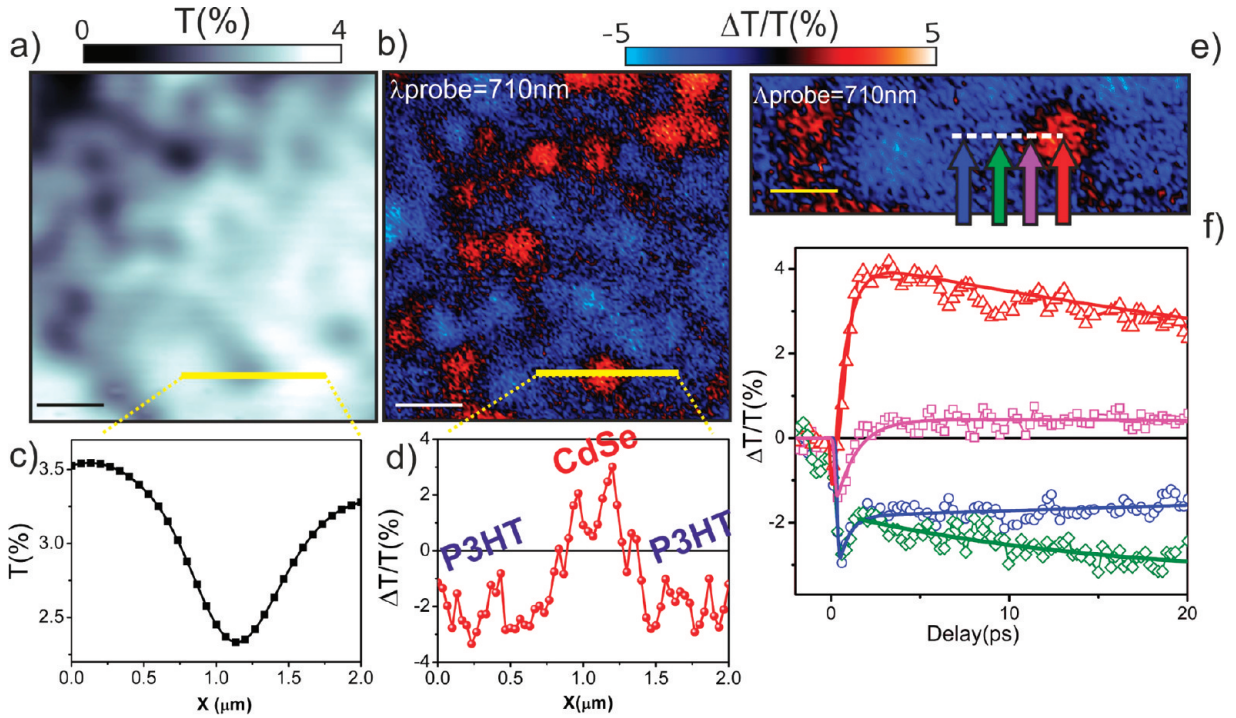

Figure 3. (a) Linear transmission map $T(x,y)$ and (b) $\Delta T/T(x,y)$ map at a τ = 1 ps pump−probe delay, simultaneously collected in the same 4 × 4 μm^2 area at a λ = 710 nm probe wavelength; scale bar = 1 μm. (c, d) Line trace profiles showing the transmission (T) and $\Delta T/T(x,y)$ signals, respectively, collected through a CdSe NC immersed in the P3HT. (e) Zoom of (b); scale bar = 500 nm. (f) $\Delta T/T(\tau)$ pump−probe dynamics corresponding to the sample positions indicated by the arrows.

We consider a type-II interface between P3HT and CdSe branches, as shown in the inset of Figure 1b.[16]

The CdSe dendritic structure is responsible for an intricate energy landscape due to carrier quantum confinement effects in both the CdSe seed and branches. To disentangle the various contributions to the excited-state dynamics in this system, we thus measure the ultrafast evolution of the $\Delta T/T(\lambda,\tau)$ signals in the visible/near-infrared regions from photoexcited carriers (averaged over a ∼150 μm spot)[22,23] both in pure CdSe NC films and in the P3HT/CdSe blend.

Figure 2a shows $\Delta T/T(\lambda)$ spectra of the pure NC at selected time delays. Upon photoexcitation with a pump pulse centered at 400 nm wavelength (3.1 eV photon energy), two positive peaks at around 560 and 670 nm appear after ultrafast thermalization in the excited state occurs within our temporal resolution (∼150 fs). They are assigned to photobleaching (PB_1 and PB_2, respectively) due to state filling in both CdSe seeds and branches. At lower energies (700−750 nm wavelengths), a short-lived ($\tau \approx 1$ ps) negative signal appears due to photoinduced absorption (PA) possibly originating from the Stark shift effect (the peak exhibits the characteristic derivative shape). Its temporal evolution is highlighted in the $\Delta T/T(\tau)$ dynamics at 710 nm plotted in red in Figure 2b. This behavior is commonly found in NCs and is attributed to a lack of symmetry in the hot carrier distribution at short delays in the NC seed.[24,25] More recently, it emerged that this feature is more correctly assigned as a signature of biexciton formation, as discussed in ref 18. The inset of Figure 2a presents the energy level diagram and the involved transitions according to our data. Photogenerated carriers in the CdSe branches relax toward the lower excited state within few hundred femtoseconds and then cross to the inner seed, where they remain trapped. In Figure 2b, we report the temporal dynamics of the $\Delta T/T(\tau)$ signals at selected wavelengths (data points) together with fits obtained using a simple rate equation model (solid lines). We see that the two positive bands exhibit different dynamics; (i) PB_1 signal at 550 nm (blue squares in Figure 2b) is formed instantaneously (within our temporal resolution) and decays biexponentially, with a fast (with $\tau_{dec} \cong 1$ ps time constant) and a slow (>10 ps) component; (ii) PB_2 at 660 nm (green circles) on the other hand is clearly delayed, showing a rise with a $\tau_{form} \cong 1$ ps time constant, followed by a slower decay. According to the matching between the fast decay component of PB_1 and the formation time of PB_2, we assign this dynamics to the population transfer from the branches to the seed, as indicated by the black dashed arrow in the energy level diagram of Figure 2a. In the near-IR region, the long-lived PA band has been generally assigned to hole trapping at the CdSe surface.[26] In our case, this PA signal becomes negligible at long times, possibly due to a low surface to volume ratio in the hyperbranched structure compared to small zero-dimensional dots.[26]

By placing P3HT in intimate contact with CdSe NC, a direct electronic interaction is established.[27,28] The ultrafast pump−probe spectroscopic measurements on the P3HT/CdSe NC (1:1) hybrid system are shown in Figure 2c. At 400 nm excitation wavelength, we estimate that both the P3HT and the CdSe NC are equally excited (50/50%). At first glance, the pump−probe spectrum resembles the pure CdSe NC one. However, two important and informative differences emerge at a deeper analysis. First of all, an additional PA band appears in the near-IR (800−900 nm) wavelength region, which is long-lived (see black triangles in Figure 2d), decaying beyond our temporal window. We attribute this component to a PA signal from delocalized holes over the two-dimensional lamellae in the ordered P3HT phase, after electron/hole separation has

dx.doi.org/10.1021/jz3000382 | J. Phys. Chem. Lett. 2012, 3, 517−523

occurred at the P3HT/CdSe interface.[29,30] Another major difference of the blend with respect to the pure material is found in the PB_1 signal dynamics; though exhibiting the same initial fast (τ_{dec} = 1 ps) decay component, the subsequent decay is considerably slower, actually beyond our temporal window. While the initial decay is reasonably due to branch to seed localization as in the neat CdSe sample, namely, arm to seed localization, the long-lived PB component could be associated with the formation of an electron−hole complex at the interface between the P3HT and the CdSe branches. The formation of this complex would hinder further capture of the electron into the CdSe seeds.

To obtain a deeper understanding of the local photophysics around the NC, we performed further measurements using the ultrafast microscopy technique, allowing simultaneously high temporal (∼150 fs) and diffraction-limited spatial (∼300 nm) resolution.[21,31,32] In a single collected image, we could distinguish the TA dynamics arising from pure CdSe NC regions from crystalline P3HT phases and from the peculiar interfacial region between the two components. Figure 3 shows the linear transmission $T(x,y)$ map (panel a) and the simultaneously collected nonlinear differential transmission $\Delta T/T$ map (b), over a 4 × 4 μm^2 area, for probe delay τ = 1 ps and wavelength λ = 710 nm. This near-IR spectral region was chosen because it allows us to discriminate between the PB_2 signal from CdSe and the PA signal from P3HT region. The linear $T(x,y)$ map reveals the micrometer-scale phase-separated morphology, present in the whole scanned sample. We assign the domain exhibiting a negligible transmission signal (darker in Figure 3a) to the CdSe-rich region, which absorbs most of the incident light. By comparing the transmission image with the $\Delta T/T$ map, we could relate the presence of the positive signal to the CdSe-rich region (red in Figure 3b), immersed in a negative signal (blue in the map) attributed to the P3HT-rich network. Figure 3c and d displays the relative intensity profile, indicating the amplitude T and the sign of the $\Delta T/T$ signal in correspondence to different morphological structures, supporting the previous assignment. By locally collecting time traces along a path connecting the CdSe NC with the P3HT rich phase, the $\Delta T/T$ signal changes from positive to negative.

In particular, the dynamics collected at the CdSe-rich phase (red triangles and pink squares in Figure 3f) show an initial negative component due to the Stark effect, which rapidly gives rise to a long-lived positive component related to residual CdSe PB_2.

This assignment agrees with the results singled out from $\Delta T/T(x,y)$ measurements (results are shown in Figure 3b and e), where the major contribution at around 710 nm comes from CdSe PB_2. Figure 4a shows the possible photophysical process occurring when the CdSe NC are excited at the focus of the confocal spot. The excitons generated in the CdSe branch yield the PB_2 signal. The subsequent exciton dissociation generates a hole in the P3HT phase and an electron in the CdSe NC. The former contributes to an amplitude reduction of the PB_2 signal in the first 10 ps time window of about the 20% with respect to the peak value at zero time delay (see red trace in Figure 3f). Note that in the averaged TA measurements in the pure CdSe NC (see Figure 2b), no decrease of the PB_2 signal was observed. Moving with the confocal spot deep toward the P3HT-rich phase, the TA maps reveal a negative signal that we assign mainly to charge pairs generated in the P3HT phase, as shown by the blue dynamics in Figure 3f. Instead, focusing at

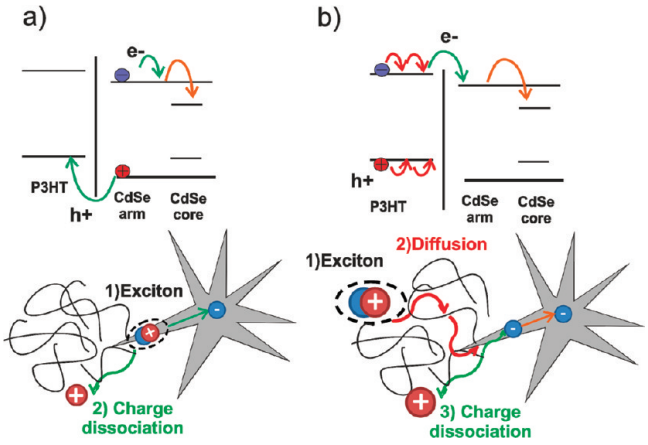

Figure 4. Cartoon of the energy level diagrams and photophysical mechanisms of charge dissociation at the hybrid P3HT/CdSe interface following photoexcitation in the (a) CdSe NC and in the (b) P3HT-rich phase .

the interface with the NC (as indicated by the green arrow in Figure 3e), the dynamics is markedly different, especially at longer times. Indeed, the signal grows negative with a time constant of $t \approx 10$ ps (see the green data diamonds and the solid fit line in Figure 3f). Such a peculiar dynamics is averaged out and essentially lost in the standard pump−probe configuration. The physical processes occurring at the interface between the long branch of the NC and the polymer phase are explained in the sketches in Figure 4b. Excitons are generated in the extended polymer phase and then gradually diffuse to the hybrid interface. Considering a typical diffusion coefficient of $D = 10^{-3}-10^{-4}$ cm^2/s,[33] the exciton diffuses for approximately 60 nm in $t \approx 10$ ps, which is comparable to the confocal spot size. At the interface, the exciton dissociates, leaving a positive charge in the P3HT, which yields the growing negative band at 710 nm, and injecting an electron into the CdSe branch. According to the results averaged on a larger area, part of these electrons will relax to the CdSe spherical seed, while the remaining electrons will form an interfacial electron−hole complex. Our results suggest that the CdSe branch is a special site for charge separation.

Efficient charge generation at the interfacial region between the larger domains is also demonstrated by measuring the work function (WF) with nanometer-scale resolution. Figure 5 shows the AFM and the relative WF image of a ITO/P3HT/CdSe blend recorded under dark and white light illumination conditions with a scanning kelvin force microscope (SKFM), enabling us to measure the photoinduced surface photovoltage with a lateral resolution higher than 100 nm.

In particular, with SKFM, it has been possible to detect the difference between the WF of the conductive tip and the local surface potential. The measurements are performed in air and involve an amplitude modulation technique in single-pass mode. Further details about the SKFM experiment are reported in the Supporting Information. In Figure 5a, two phases with relatively large size, as already observed by the linear transmission confocal imaging (see Figure 3a), can be clearly distinguished, one P3HT-rich (the darker phase on the colored z-scale, labeled as "1") and the other NCs-rich (the whiter phase on the colored z-scale, labeled as "2"). The height contrast between the two phases is about 60 nm. In dark conditions (see Figure 5c), the potential difference between the two phases is very small; the surface potential distribution (see

dx.doi.org/10.1021/jz3000382 | J. Phys. Chem. Lett. 2012, 3, 517−523

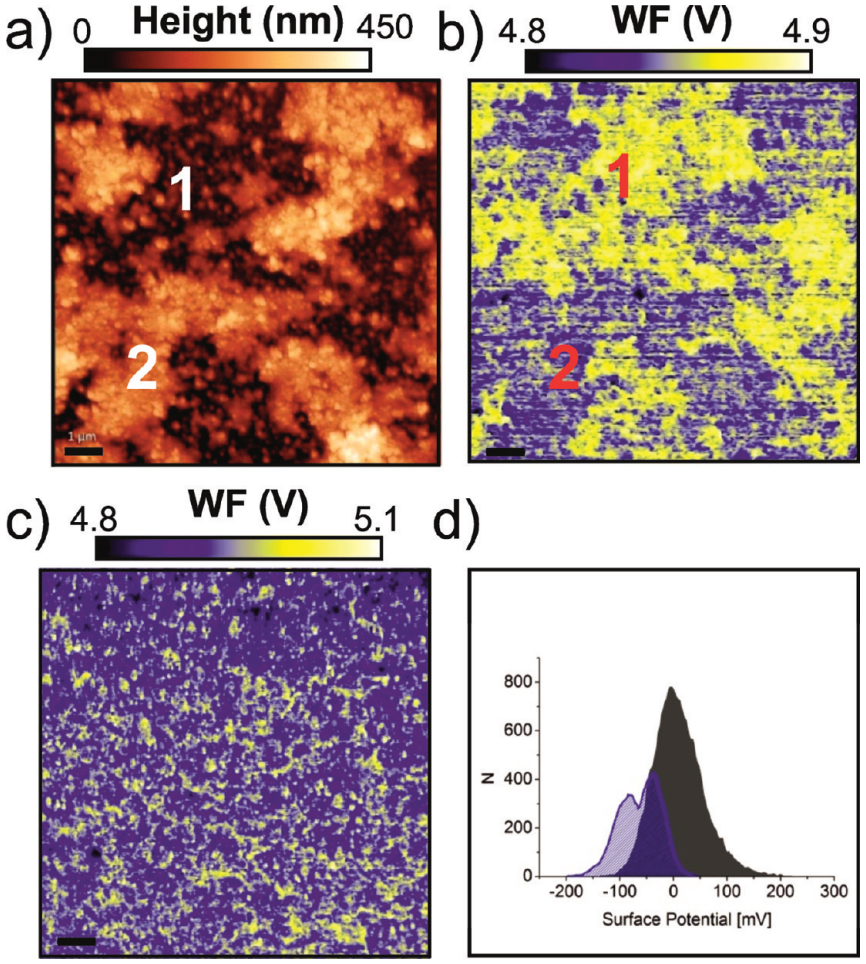

Figure 5. (a) Topography of a 1:1 (w/w) P3HT/CdSe blend. (b) WF in the same area of (a) under white light illumination and (c) in the dark; scale bar = 1 μm. (d) Histogram distributions of the surface potential images measured on a P3HT/CdSe hyperbranched blend, showing the relative number of pixels with a given WF detected on a single 10 μm × 10 μm area. Black and blue solid lines represent the measurements under dark and light conditions, respectively.

Figure 5d) has the maximum peak centered close to 0. In an ideal case, the surface potential measured in the darkness should be equal to the WF difference between the tip and the ITO bottom electrode. In our experiment, we have a Ti−Pt tip with a measured WF of $\varphi_{tip} = 4.8 \pm 0.02$ eV, while the ITO WF is $\varphi_{ITO} \approx 4.7-4.8$ eV, in accord with values reported in the literature.[34] However, under illumination (see Figure 5b), we do observe a more negative potential in all regions with respect to the values of the potential measured in the dark. The shift toward lower surface potential values, switching upon illumination, indicates an excess of electrons. These measurements reveal that efficient charge separation occurs both at the distributed heterojunctions present in the fine-scale phase-separated polymer/NC regions and at the interface between macro P3HT/NC phases.

In conclusion, combining pump−probe, ultrafast microscopy, and SKFM, we obtained a quite complete picture of the charge carrier photogeneration in a hyperbranched NC/polymer composite. We found that the expected charge separation is enhanced at the extreme of the branches, pointing from the seed to the polymer. Charge separation occurs quickly if the exciton is generated in the CdSe branch in direct contact with the P3HT phase. However, it becomes delayed when the exciton is generated within the extended P3HT phase as the exciton must diffuse before encountering the hybrid interface site for charge separation.

These results confirm the primary role of the highly branched CdSe geometry in forming a nanoscale morphology with the polymer, leading to the creation of a high interfacial area and an effective percolation network for electrons, fundamental requirements to achieve for efficient hybrid devices. However, we also evidenced strong trapping dynamics of photogenerated charges in the large spherical core seeds, which show clear spectral features both in the absorption and in the TA measurements. Furthermore, we found that a considerable fraction of the NC volume consists of large spherical seeds, thus making the carrier trapping relevant in preventing efficient free charge percolation to the electrodes. We envisage that the growth of a highly connected structure of long branches without the presence of a large amount of bulky spherical seed cores would be beneficial for efficient charge percolation and transport in optimized hybrid devices. Possibly, a suitable choice of the material composing the seed could allow one to engineer the branch−seed interface. In particular, a large gap would hamper carrier decay into the seed, providing long-lived carriers and a larger hopping yield while preserving the advantage of the sea urchin shape in the percolation network.

dx.doi.org/10.1021/jz3000382 | J. Phys. Chem. Lett. 2012, 3, 517−523

EXPERIMENTAL METHODS

In a typical pump−probe experiment, the system under study is photoexcited by a short pump pulse, and its subsequent dynamical evolution is detected by measuring the differential transmission changes $\Delta T(\tau,\lambda)$ of a delayed probe pulse as a function of pump−probe delay τ and probe wavelength λ. The signal is given by the differential transmission $\Delta T/T = [(T_{pumpon} - T_{pumpoff})/T_{pumpoff}]$. The pump−probe setup is driven by 1 kHz repetition rate pulse train at λ = 780 nm (central wavelength) with a 150 fs duration coming from a regeneratively amplified mode-locked Ti:Sapphire laser (Clark-MXR Model CPA-1).[23] The pump pulse is produced at a 390 nm wavelength by second harmonic generation, while the probe is a white light continuum spanning the 450−800 nm range. By pumping the sample at 3.1 eV (400 nm) at low pump fluence (E = 1 μJ/cm^2), we mainly excite electrons from the valence band to the conduction band of the CdSe branches.

The ultrafast transient absorption microscope is based on a homemade confocal microscope combined with an ultrafast pump−probe system, similar to the one previously described. The pump and probe beams are coupled in the microscope objective used both for focusing and collection. Working in a standard epi-configuration, the collected probe is then focused on the core of an optical fiber, used as the confocal pinhole, and detected. By raster scanning the sample position (x,y) with a piezo-translator and by changing the pump−probe delay (τ) with a motorized delay stage, we simultaneously acquire three-dimensional linear transmission $T(x,y,\lambda)$ images and 4D differential transmission $\Delta T/T(x,y,\lambda,\tau)$ images.[31,32] Further details can be found in the Supporting Information. We collect $\Delta T/T(x,y)$ images of the sample at a selected probe wavelength and fixed pump−probe delay, and we measure the temporal dynamics $\Delta T/T(\tau)$ at a fixed sample position.

ASSOCIATED CONTENT

Supporting Information

Experimental setup, sample preparation details, additional pump−probe spectra, and the confocal map. This material is available free of charge via the Internet at http://pubs.acs.org.

AUTHOR INFORMATION

Corresponding Author

*E-mail: giulia.grancini@iit.it (G. Grancini); francesco.scotognella@polimi.it (F. Scotognella).

Notes

The authors declare no competing financial interest.

ACKNOWLEDGMENTS

The authors acknowledge financial support through the Projects PITN-GA-2009-237900 (ICARUS) and FP7-ICT-248052(PHOTOFET). This work was supported by the Italian projects Rete Nazionale di Ricerca sulle Nanoscienze ItalNanoNet (FIRB Reference Number RBPR05JH2P), EFOR-Energia da Fonti Rinnovabili (Iniziativa CNR per il Mezzogiorno L. 191/2009 art. 2 comma 44), and European Project, ESCORT (Efficient Solar Cells based on Organic and hybrid Technology). The authors thank Prof. G. Cerullo for helpful discussion.

REFERENCES

(1) Dayal, S.; Kopidakis, N.; Olson, D. C.; Ginley, D. S.; Rumbles, G. Photovoltaic Devices with a Low Band Gap Polymer and CdSe Nanostructures Exceeding 3% Efficiency. *Nano Lett.* **2010**, *10*, 239−242.

(2) Greenham, N. C.; Peng, X.; Alivisatos, A. P. Charge Separation and Transport in Conjugated−Polymer/Semiconductor−Nanocrystal Composites Studied by Photoluminescence Quenching and Photoconductivity. *Phys. Rev. B* **1996**, *54*, 17628−17637.

(3) Saunders, B. R.; Turner, M. L. Nanoparticle−Polymer Photovoltaic Cells. *Adv. Colloid Interface Sci.* **2008**, *138*, 1−23.

(4) Sun, B. Q.; Snaith, H. J.; Dhoot, A. S.; Westenhoff, S.; Greenham, N. C. Vertically Segregated Hybrid Blends for Photovoltaic Devices with Improved Efficiency. *J. Appl. Phys.* **2005**, *97*, 014914−014919.

(5) Dennler, G.; Scharber, M. C.; Brabec, C. J. Polymer−Fullerene Bulk-Heterojunction Solar Cells. *Adv. Mater.* **2009**, *21*, 1323−1338.

(6) Clarke, T. M.; Durrant, J. R. Charge Photogeneration in Organic Solar Cells. *Chem. Rev.* **2010**, *110*, 6736−6767.

(7) Lewis, N. S. Toward Cost-Effective Solar Energy Use. *Science* **2007**, *315*, 798−801.

(8) Sun, B. Q.; Marx, E.; Greenham, N. C. Photovoltaic Devices Using Blends of Branched CdSe Nanoparticles and Conjugated Polymers. *Nano Lett.* **2003**, *3*, 961−963.

(9) Kanaras, A. G.; Sonnichsen, C.; Liu, H.; Alivisatos, A. P. Controlled Synthesis of Hyperbranched Inorganic Nanocrystals with Rich Three-Dimensional Structures. *Nano Lett.* **2005**, *5*, 2164−2167.

(10) Han, L.; Qin, D.; Jiang, X.; Liu, Y.; Wang, L.; Chen, J.; Cao, Y. Synthesis of High Quality Zinc-Blende CdSe Nanocrystals and Their Application in Hybrid Solar Cells. *Nanotechnology* **2006**, *17*, 4736−4742.

(11) Gur, I.; Fromer, N. A.; Chen, C.; Kanaras, A. G.; Alivisatos, A. P. Hybrid Solar Cells with Prescribed Nanoscale Morphologies Based on Hyperbranched Semiconductor Nanocrystals. *Nano Lett.* **2007**, *7*, 409−414.

(12) Liu, J. S.; Tanaka, T.; Sivula, K.; Alivisatos, A. P.; Frechet, J. M. J. Employing End-Functional Polythiophene To Control the Morphology of Nanocrystal−Polymer Composites in Hybrid Solar Cells. *J. Am. Chem. Soc.* **2004**, *126*, 6550−6551.

(13) Huynh, W. U.; Dittmer, J. J.; Alivisatos, A. P. Hybrid Nanorod−Polymer Solar Cells. *Science* **2002**, *295*, 2425−2427.

(14) Sun, B.; Greenham, N. C. Improved Efficiency of Photovoltaics Based on CdSe Nanorods and Poly(3-hexylthiophene) Nanofibers. *Phys. Chem. Chem. Phys.* **2006**, *8*, 3557−3560.

(15) Xu, J.; Wang, J.; Mitchell, M.; Mukherjee, P.; Jeffries-EL, M.; Petrich, J. W.; Lin, Z. Organic−Inorganic Nanocomposites via Directly Grafting Conjugated Polymers onto Quantum Dots J. *Am. Chem. Soc.* **2007**, *129*, 12828−12833.

(16) Li, Y.; Mastria, R.; Fiore, A.; Nobile, C.; Yin, L.; Biasiucci, M.; Cheng, G.; Cucolo, A. M.; Cingolani, R.; Manna, L.; Gigli, G. Improved Photovoltaic Performance of Heterostructured Tetrapod-Shaped CdSe/CdTe Nanocrystals Using C60 Interlayer. *Adv. Mater.* **2009**, *21*, 4461−4466.

(17) Kambhampati, P. Unraveling the Structure and Dynamics of Excitons in Semiconductor Quantum Dots. *Acc. Chem. Res.* **2011**, *44*, 1−13.

(18) Kambhampati, P. Hot Exciton Relaxation Dynamics in Semiconductor Quantum Dots: Radiationless Transitions on the Nanoscale. *J. Phys. Chem. C* **2011**, *115*, 22089−22109.

(19) Scotognella, F.; Miszta, K.; Dorfs, D.; Zavelani-Rossi, M.; Brescia, R.; Marras, S.; Manna, L.; Lanzani, G.; Tassone, F. Ultrafast Exciton Dynamics in Colloidal CdSe/CdS Octapod Shaped Nanocrystals. *J. Phys. Chem. C* **2011**, *115*, 9005−9011.

(20) Fiore, A.; Mastria, R.; Lupo, M. G.; Lanzani, G.; Giannini, C.; Carlino, E.; Morello, G.; Giorgi, M. D.; Li, Y. Q.; Cingolani, R.; Manna, L. Tetrapod-Shaped Colloidal Nanocrystals of II−VI Semiconductors Prepared by Seeded Growth. *J. Am. Chem. Soc.* **2009**, *131*, 2274−2282.

(21) Grancini, G.; Polli, D.; Fazzi, D.; Cabanillas-Gonzalez, J.; Cerullo, G.; Lanzani, G. Transient Absorption Imaging of P3HT:PCBM Photovoltaic Blend: Evidence For Interfacial Charge Transfer State. *J. Phys. Chem. Lett.* **2011**, *2*, 1099−1105.

(22) Clark, J.; Lanzani, G. Organic Photonics for Communications. *Nat. Photonics* **2010**, *4*, 438−446.
(23) Lanzani, G.; Cerullo, G.; Polli, D.; Gambetta, A.; Zavelani-Rossi, M.; Gadermaier, C. Photophysics of Conjugated Polymers: The Contribution of Ultrafast Spectroscopy. *Phys. Status Solidi A* **2004**, *201*, 1116−1131.
(24) Malko, A. V.; Mikhailovsky, A. A.; Petruska, M. A.; Hollingsworth, J. A.; Klimov, V. I. Interplay between Optical Gain and Photoinduced Absorption in CdSe Nanocrystals. *J. Phys. Chem. B* **2004**, *108*, 5250−5255.
(25) Rath, M. C.; Mondal, J. A.; Palit, D. K.; Mukherjee, T.; Ghosh, H. N. Femtosecond Transient Absorption Studies in Cadmium Selenide Nanocrystal Thin Films prepared by Chemical Bath Deposition Method. *J. Nanomater.* **2007**, *2007*, 36271−36277.
(26) Tyagi, P.; Kambhampati, P. False Multiple Exciton Recombination and Multiple Exciton Generation Signals in Semiconductor Quantum Dots arise from Surface Charge Trapping. *J. Chem. Phys.* **2011**, *134*, 094706/1−10.
(27) Sykora, M.; Petruska, M. A.; Alstrum-Acevedo, J.; Bezel, I.; Meyer, T. J.; Klimov, V. I. Photoinduced Charge Transfer between CdSe Nanocrystal Quantum Dots and Ru−Polypyridine Complexes. *J. Am. Chem. Soc.* **2006**, *128*, 9984−9985.
(28) Heinemann, M. D.; von Maydell, K.; Zutz, F.; Kolny-Olesiak, J.; Borchert, H.; Riedel, I.; Parisi, J. Photo-induced Charge Transfer and Relaxation of Persistent Charge Carriers in Polymer/Nanocrystal Composites for Applications in Hybrid Solar Cells. *Adv. Funct. Mater.* **2009**, *19*, 3788−3795.
(29) Guo, J.; Ohkita, H.; Benten, H.; Ito, S. Near-IR Femtosecond Transient Absorption Spectroscopy of Ultrafast Polaron and Triplet Exciton Formation in Polythiophene Films with Different Regioregularities. *J. Am. Chem. Soc.* **2009**, *131*, 16869−16880.
(30) Korovyanko, O. J.; Österbacka, R.; Jiang, X. M.; Vardeny, Z. V.; Janssen, R. A. J. Photoexcitation Dynamics in Regioregular and Regiorandom Polythiophene Films. *Phys. Rev. B* **2001**, *64*, 235122−235127.
(31) Polli, D.; Grancini, G.; Clark, J.; Celebrano, M.; Virgili, T.; Cerullo, G.; Lanzani, G. Nanoscale Imaging of the Interface Dynamics in Polymer Blends by Femtosecond Pump−Probe Confocal Microscopy. *Adv. Mater.* **2010**, *22*, 3048−3051.
(32) Cabanillas-Gonzalez, J.; Grancini, G.; Lanzani, G. Pump−Probe Spectroscopy in Organic Semiconductors: Monitoring Fundamental Processes of Relevance in Optoelectronics. *Adv. Mater.* **2011**, *23*, 5468−5485.
(33) Cabanillas-Gonzalez, J.; Gambetta, A.; Zavelani-Rossi, M.; Lanzani, G. Kinetics of Interfacial Charges in Hybrid GaAs/Oligothiophene Semiconducting Heterojunctions. *Appl. Phys. Lett.* **2007**, *91*, 122113−122115.
(34) VanSlyke, S. A.; Chen, C. H.; Tang, C. W. Organic Electroluminescent Devices with Improved Stability. *Appl. Phys. Lett.* **1996**, *69*, 2160−2162.